Available online at www.sciencedirect.com
ScienceDirect
Journal of Molecular Catalysis A: Chemical 265 (2007) 80–89
JOURNAL OF MOLECULAR CATALYSIS A: CHEMICAL
www.elsevier.com/locate/molcata

Hydrodechlorination reactivity of *para*-substituted chlorobenzenes over platinum/carbon catalyst

Tetsuya Yoneda [a,*], Toshio Takido [b], Kenji Konuma [a]

[a] *College of Science and Technology, Nihon University, Narashinodai 7-24-1, Funabashi, Chiba 274-8501, Japan*
[b] *College of Science and Technology, Nihon University, Kanda-Surugadai 1-8-14, Chiyoda, Tokyo 101-8308, Japan*

Received 10 February 2006; received in revised form 23 September 2006; accepted 27 September 2006
Available online 4 October 2006

Abstract

In order to clarify the factors that affect the hydrodechlorination (abbreviated as HDC) reactivity of aromatic chlorinated compounds, the catalytic hydrotreatment of chlorobenzene (abbreviated as CLB) and *para*-amino, -methoxy, -methyl, -chloro, -trifluoromethyl, -acetyl, and -cyano-substituted chlorobenzenes (abbreviated as CLAN, CLAS, CLTN, DCLB, CLTF, CLAP and CLBN, respectively) was carried out over 5%-platinum/carbon (Pt/C) catalyst under 1 MPa of hydrogen pressure at 523 K.

In the HDC of CLB and the substituted chlorobenzenes, except for CLBN and CLAP, reductive cleavage between the chlorine atom and the carbon atom took place selectively. In the case of CLBN and CLAP, in contrast, hydrogenolysis of the substituent in the *para*-position occurred preferentially. In the course of the reaction of CLBN, furthermore, secondary bi-molecular condensation of the hydrogenated intermediate occurred and an appreciable amount of bis(4-chlorobenzyl)amine was produced.

HDC reactivity of the chlorobenzenes with electron-donating substituents decreased in the order of CLAN $\gg$ CLAS $\geq$ CLTN $\geq$ CLB. This order of the Pt/C catalyst was similar to that of a 5%-palladium/carbon (Pd/C) catalyst, which has been reported previously. On the other hand, the reactivity of the chlorobenzenes with electron-withdrawing substituents decreased in the order of CLB $\geq$ DCLB $\gg$ CLTF. This behavior is in contrast with that observed on the Pd/C catalyst. In the molecular orbital calculation using the DFT method (B3LYP/LANL2DZ), except for CLBN, CLAP and CLTF, the most stable point was obtained when the chlorobenzenes were adsorbed through the chlorine atom on the corner platinum atom of the Pt_{14} model cluster. For CLTF, adsorption on the corner platinum atom seemed to occur through the trifluoromethyl substitution in the *para*-position. The magnitude of the adsorption energy (absolute value) decreased in the following order: CLAN $\gg$ CLAS $\geq$ CLTN $\geq$ CLB > DCLB $\gg$ CLTF. This order of adsorption energy was in good agreement with that of HDC reactivity. The reasons for the adsorption stability are discussed from the viewpoint of the energy level of the frontier orbital.

Keywords: Hydrodechlorination; *Para*-substituted chlorobenzenes; Platinum/carbon catalyst; Molecular orbital calculation; Adsorption energy

1. Introduction

Since most chlorinated compounds used in the chemical industry are toxic to human being, treatment to render them harmless is crucial in maintaining a clean natural environment. Many treatment methods have been studied, such as catalytic hydrogenolysis [1–35], ultraviolet-ray degradation [36–40], ultrasonic irradiation [20,41], electrolysis [42,43], biological disposal [41,44] and others [45–47]. Among these, catalytic hydrogenolysis appears to be the safest because it does not generate other toxic compounds such as dioxin as by-products [1,2,5,14–17].

Studies on catalytic hydrogenolysis can be classified into two groups: one group is the gas phase reactions with bulk or supported Fe [8], Co [8], Ni [1–11], Pt [30,31], Pt–V [31], Pt–Mo [31] and Pt–W [31], and the other group is the liquid phase reactions with bulk or supported Ni–Mo [13,14], Ni [15,16], Raney-Ni [16,26], Pd [11,17–28], Pd–Ru [29], and Pt [32–35].

However, most reports on hydrodechlorination (HDC) so far have focused on catalytic preparation, catalytic characteristics and/or catalytic activity, reaction path and/or mechanism, and the effect of additives. Few papers have dealt with the HDC reactivity of reactants from the standpoint of the electronic effect of the substituents [1,3,9–11,16,19].

* Corresponding author. Tel.: +81 47 469 5310.
E-mail address: yoneda@chem.ge.cst.nihon-u.ac.jp (T. Yoneda).

1381-1169/$ – see front matter © 2006 Elsevier B.V. All rights reserved.
doi:10.1016/j.molcata.2006.09.044

Suzdorf et al. [1] studied the gas phase HDC of chlorobenzene and *ortho*-, *meta*- and/or *para*-isomers of dichlorobenzene, chlorotoluene, chloroaniline and chlorobenzene trifluoride on Ni/γ-Al_2O_3, and showed a correlation between HDC reactivity and Hammett's substitution constant. Also in the gas phase HDC of chlorobenzene, chlorotoluenes, chlorophenols, dichlorobenzenes and trichlorobenzenes on Ni/SiO_2 catalyst, Keane and co-workers [3,9–11] reported that the presence of an electron-donating ring substituent enhanced HDC where a cationic intermediate is stabilized by an electron-donating substituent on the Ni catalyst and accelerates the reaction rate. Wu et al. [16] reported that under liquid phase HDC of three (*ortho*-, *mete*- and *para*-) isomers of chlorotoluenes, chloroanilines, chlorobenzene trifluorides, dichlorobenzenes, and two isomers (1,2,3- and 1,2,4-) trichlorobenzenes over Ni/C, Ni/γ-Al_2O_3, Ni/SiO_2 and Raney-Ni, in the presence of alkaline hydroxide, chlorobenzene derivatives having either an electron-donating or an electron-withdrawing group showed a decreased HDC reactivity. On the other hand, in our previous study on the liquid phase reaction of chlorobenzene and *para*-isomers of chloroaniline, chloroanisole, chlorotoluene, dichlorobenzene, chloroacetophenone and chlorobenzonitrile on the Pd/C catalyst [19], the HDC reactivity of these substituted chlorobenzenes was accelerated by the presence of substituents, and a good relationship was observed between the reactivity and Hammett's constant. Although these results on HDC reactivity are very useful from academic and practical standpoints, a direct comparison of reactivity is impossible because these studies were carried out under different reaction conditions. Hence, detailed information on the factors affecting HDC reactivity is not readily available.

In order to shed light upon the factors affecting the HDC reactivity of chlorinated aromatic compounds, in the present study, the HDC reaction rate of chlorobenzene (abbreviated as CLB) and the *para*-amino, -methoxy, -methyl, -chloro, -trifluoromethyl, -acetyl and -cyano-substituted chlorobenzenes (abbreviated as CLAN, CLAS, CLTN, DCLB, CLTF, CLAP and CLBN, respectively) was measured over a 5%-Pt/C catalyst in conditions similar to those of the previous reactions on the Pd/C catalyst [19]. Furthermore, the adsorption energy of the chlorobenzenes on the model cluster of the Pt_{14} unit cell was calculated using the molecular orbital method (DFT method), and experimental results were discussed from the viewpoint of adsorption stability.

2. Experimental

2.1. Materials

Chlorobenzene, the *para*-isomers of CLTN, DCLB, and CLBN, and solvents of hexadecane and 1,3,5-trimethylbenzene were obtained from Kanto Kagaku Co. CLAN, CLAS, CLAP and CLTF were purchased from Tokyo Kasei Kogyo Co., Ltd. These substrates were purified according to the conventional method before use.

5%-Pt/C, which was supplied by Nippon Engelhard Inc., was used without purification. The particle size of the catalyst was less than 45 μm (>330 mesh).

2.2. Apparatus

The HDC reaction was carried out in a test tube (Pyrex glass, i.d. 28 mm × height 130 mm, volume: ca. 74 ml) that was placed into a magnetically stirred autoclave (Sakashita Seisakusho, SUS304, volume: ca. 108 ml) equipped with a sampling tube (SUS316, i.d. 0.25 mm × length 900 mm) and a liquid introducing vessel (SUS304, volume: 50 ml).

In order to maintain effective agitation of the reactants, three rectangular turbulence boards (length 60 mm × width 4 mm × thickness 1.5 mm, glass) were fusion-bonded on the inner wall of the test tube with three points that were divided equally on the inner circumference.

Except for the improved test tube, the details of the apparatus were described in the previous paper [19].

2.3. Procedure

The Pt/C catalyst (0.0100 g) was placed into the test tube in the autoclave. After purging the air of the autoclave with hydrogen gas, the catalyst was reduced in a hydrogen flow rate of 100 ml/min under 0.5 MPa at 573 K for 1 h. Upon the termination of the catalyst reduction, the residual hydrogen gas in the autoclave was rapidly released, and hexadecane as a solvent was added from the liquid introducing vessel into the autoclave using 0.3 MPa hydrogen. Then, the pressure in the reactor was adjusted to 0.5 MPa at 558 K, and both the solvent and the catalyst were stirred at 500 rpm.

The temperature of the reactor was maintained at 523 K, and 1,3,5-trimethylbenzene (5 ml) solution of reactant (final concentrations in the reaction: $(25–100) \times 10^{-3}$ mol/l) was then added from the liquid introducing vessel using hydrogen of ca. 0.8 MPa, following pressure adjustment to 1 MPa. In the course of the reaction, hydrogen pressure and temperature were kept at 1.0 ± 0.05 MPa and 523 ± 1 K, respectively. Except for DCLB, the starting Cl(mol)/Pt(g) ratios were in the range of ca. 2–8 mol/g. For DCLB that possesses two chlorine atoms in the molecule, the ratio was in the range of ca. 4–16 mol/g.

The reaction time was set at zero, when the reactant solution was introduced into the reactor. During the course of the reaction, the products were taken periodically through the sampling tube.

2.4. Analysis

The reaction products were analyzed by a gas chromatograph (Shimadzu GC-14A or 14B) using wide bore capillary columns (Varian CP-Sil 13CB: i.d. 0.53 mm × length 100 m, or Varian CP-Wax 52CB: i.d. 0.53 mm × length 60 m) equipped with an FID detector. Identification was carried out by gas chromatography–mass spectroscopy (Shimadzu GC–MS5050QA) using a narrow bore capillary column (J&W Scientific DB-1: i.d. 0.25 mm × length 60 m). In the quantitative analysis, toluene or *meta*-xylene was used as the internal standard.

The initial reaction rates were determined by plotting the concentration of the HDC product versus the reaction time. Power series with the third order ($r = at^3 + bt^2 + ct$) were applied to these

plotted data, and the initial reaction rate was determined as the differential coefficient of the power series at $(dr/dt)_{t=0}$. That is the coefficient of the first order term.

For Pt/C catalyst characterization, the metal content was measured by a UV–vis spectrophotometer (U-2010, Hitachi Inc.) from the diluted dissolution in aqua regia and the dry ashing. BET surface areas and pore size distribution were determined using a BELSORP-mini (BEL Japan Inc.) apparatus. After outgasing at 393 K, nitrogen adsorption isotherm was employed to determine the total surface area using the standard multiple point BET method at 77 K. Mesopore and micropore volumes were measured according to the BJH method and the MP or *t*-plot method, based on a carbon standard curve endorsed by BEL Japan Inc. The metal surface area, dispersion, and average metal particle size were obtained from carbon monoxide (CO) chemisorption analysis (R-6015, Ohkura Riken Inc.). The samples (0.1 g each) were loaded in a U-shaped Pyrex glass cell (i.d. 3.5 mm, volume 5 ml) and reduced in hydrogen at 473 K for 15 min. After the reduction, the samples were swept with 50 ml/min dry helium for 15 min, cooled to 323 K and subjected to CO chemisorption using a pulse (30%-CO/He, 0.45 ml, four times) titration procedure in He flow (50 ml/min). Powder X-ray diffractograms (XRD) were recorded with an RU-200 instrument (RAD-RB, Rigaku Co.) using nickel filtered Cu Kα radiation. The samples were mounted in a low background sample holder and scanned at a rate of 0.02°/step over the $5 \leq 2\theta \leq 70°$ range at a scan speed of 4°/min. The diffractograms were compared with the JCPDS-PDF references (no. 4-0802) for identification purposes.

2.5. Molecular orbital calculation of model complexes

To elucidate the factors affecting the HDC reaction of *para*-substituted chlorobenzenes, both the adsorption state and the adsorption energy of the chlorobenzenes on the model cluster of the Pt_{14} unit cell were investigated by density function theory (DFT: B3LYP) [48–52], using Gaussian03W (Rev. B.04) on a Windows 2000 system. LANL2DZ [53–56] was used as the basis set.

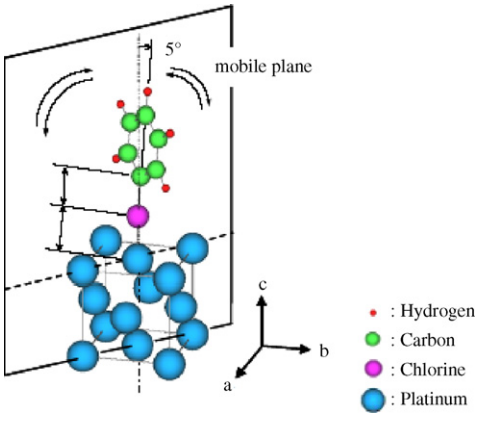

Fig. 1. A model complex of "chlorobenzene–Pt_{14}" cluster and the mobile plane of the organic part in optimization.

The convergence criteria of the maximum force, RMS force, maximum displacement and RMS displacement were 0.00045, 0.0003, 0.0018 and 0.0012 (default values), respectively. The model cluster was the Pt_{14} unit cell that was constructed by using the DV-Xα program [57]. Prior to constructing the "chlorobenzenes–Pt_{14}" complexes, the organic part of the complexes was optimized using the B3LYP/LANL2DZ system. In the initial geometry of the complexes, as seen in Fig. 1, the molecular axis of the chlorobenzenes was inclined at 5° to the right side. During the course of the optimization process of the model complexes, the geometry of the Pt_{14} cluster was fixed. In the optimization, as a result, the mobile space of the organic part in the complex was kept in the range of the (1 1 0) plane of the cluster (Fig. 1).

3. Results and discussion

3.1. Catalyst characterization

The physicochemical properties of the Pt/C catalyst is given in Table 1. The platinum particle size, *D*, has been calculated from the chemisorption results by assuming a stoichiometry CO:Pt = 1:1 and by using the equation $D = 5\ V/S$ where *V* and *S* indicate the volume and surface area of platinum, respectively. The values obtained by the CO chemisorption were used with a platinum density of 21.45 g/cm^3, atomic weight of 195.08, lattice constant of 0.3923 nm. The XRD pattern for the activated catalyst sample is given in Fig. 2. The Pt/C diffractogram is characterized by three peaks at 39.8°, 46.2°, 67.6°, corresponding to the (1 1 1), (2 0 0), and (2 2 0) planes of metallic platinum that are consistent with an exclusive cubic symmetry. The markers included in Fig. 2 illustrate the position and relative intensity of the XRD peaks for cubic Pt taken from the Powder Diffraction File (no. 4-0802) in JCPDS.

In the preliminary calculation of chlorobenzenes on the (1 1 1) plane, no reasonable interaction was observed although the intensity of the (1 1 1) plane was the highest in the XRD. Since the arrangement of the platinum atom in the (2 0 0) plane of the metal crystal is assumed to be the same as that in the

Table 1
Metal content, BET surface area and metal phase characteristics of Pt/C catalyst

	Pt/C
Metal loading (w/w, %)	4.9
BET surface area (m^2/g)	966
Mesopore volume (cm^3/g)	0.35[a], 0.36[b]
Micropore volume (cm^3/g)	0.36[c], 0.45[d]
Pore diameter (nm)[d]	0.97
CO adsorption volume (ml/g)[e]	0.74
Metal surface area (m^2/g)	3.1
Average metal particle size (nm)	3.7
Dispersion (%)	13

[a] BJH method associated with chemisorption.
[b] BJH method associated with desorption.
[c] MP method.
[d] *t*-Plot method.
[e] STP, 0.101 MPa and 273 K.

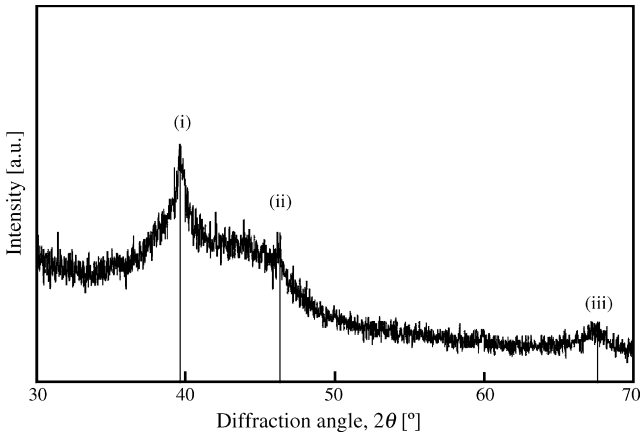

Fig. 2. X-ray diffraction pattern: diffraction angles ((i) 39.8°; (ii) 46.2°; (iii) 67.6°) connected with Pt/C catalyst.

(1 0 0) plane, as the first step to investigate the adsorption state, it is reasonable to use the (1 0 0) plane as a model plane in the molecular orbital calculation.

3.2. Hydrodechlorination (HDC)

3.2.1. Product distribution

To elucidate the electronic factors that affect HDC on a 5%-Pt/C catalyst, a series of *para*-substituted chlorobenzenes with electron-donating or -withdrawing substituents were reacted under H_2 1 MPa at 523 K.

In the HDC of CLB and *para*-substituted chlorobenzenes with electron-donating substituents (CLAN, CLAS and CLTN), reductive cleavage between the chlorine atom and the carbon atom of the benzene ring took place selectively. A very small amount of cyclohexane as ring-saturated compound was also observed only in the reaction of CLB.

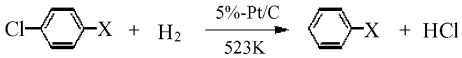

(X: NH_2, OCH_3, CH_3, H, Cl, CF_3)

Depending on the magnitude of the electronic properties of each substituent, however, the features of the reactivity of substituted chlorobenzenes with electron-withdrawing substituents differed slightly from those with electron-donating substituents. That is, hydrogenolysis of the substituent in the *para*-position occurred in the reaction of CLBN and CLAP, whereas normal HDC took place in the case of DCLB and CLTF. In the case of CLBN, as shown in Table 2, a considerable amount of bis(4-chlorobenzyl)amine was produced together with a small amount of toluene and benzonitrile. Although further study is required, from the products distribution shown in Table 2, the following reaction path may be suggested for the reaction of CLBN (Fig. 3).

As reaction products of CLAP, acetophenone and ethylbenzene were observed as shown in Table 2.

When Pd/C was used as a catalyst [19], the C–Cl bond cleavage only took place selectively in the reaction CLBN and CLAP. Such a difference in product distribution between Pt/C and Pd/C may indicate a different reaction mechanism.

3.2.2. HDC reaction rate constant

Except for CLBN and CLAP, the HDC reaction rates of the chlorobenzenes with both electron-donating and -withdrawing

Table 2
Reaction conversion and selectivity for the hydrodechlorination of chlorobenzenes[a]

Substrate	Time (min)	Product	Conversion (mol%)	Selectivity[b] (mol%)
p-Chloroaniline (CLAN)	30	Aniline	3.3	100
p-Chloroanisole (CLAS)	240	Anisole	2.7	100
p-Chlorotoluene (CLTN)	180	Toluene	1.9	100
Chlorobenzene (CLB)	180	Benezene	1.8	99.9
		Cyclohexane		<0.1
p-Dichlorobenzene (DCLB)	180	Chlororbenzene	1.6	100
p-Chlorobenzene trifluoride (CLTF)	240	Trifluoromethylbenzene	0.1	100
p-Chloroacetophenone (CLAP)	90		36.8	
		Ethylbenzene		5.4
		p-Chloroethylbenzene		69.6
		Acetophenone		10.9
		4-Chloro-α-methyl-benzylalcohol		14.1
p-Chlorobenzonitrile (CLBN)	10		75.5	
		Toluene		3.6
		Benzonitrile		<0.1
		Benzylamine		2.7
		p-Chlorobenzylamine		28.2
		Unknown[c]		13.1
		Bis(4-chlorobenzyl)amine		69.3

[a] Substrate (4×10^{-3} mol), solvent (40 ml), catalyst (0.01 g) were employed.
[b] Determined by GLC analysis using internal hydrocarbon standard (toluene or *m*-xylene).
[c] No identification by GC–MS analysis.

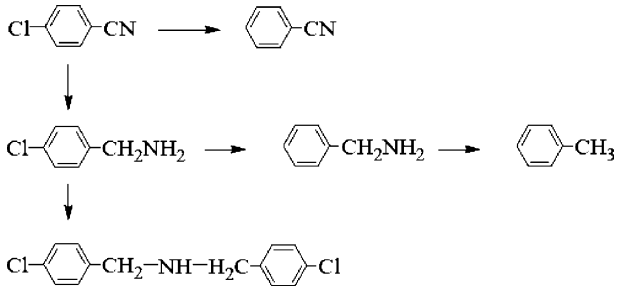

Fig. 3. Reaction paths suggested for the hydrodechlorination of *p*-chlorobenzonitrile.

substituents were proportional to the initial concentration of the reactant, and the reaction orders for the concentration of these chlorobenzenes were, respectively, in the range of 0.90–1.02 and 1.00–1.02. These results are shown in Figs. 4 and 5.

Furthermore, for the electron-donating substituents, the magnitude of the reaction rate constants decreased in the order of CLAN > CLAS ≥ CLTN ≥ CLB. This order of reactivity, or the rate constant, on the Pt/C catalyst is agreement with that on the Pd/C catalyst reported previously [19], and suggests that the reactivity of these substituted chlorobenzenes was accelerated by the presence of electron-donating substituents.

However, in the case of chlorobenzenes with electron-donating substituents, except for CLBN and CLAP, the rate constant decreased in the following order: CLB ≥ DCLB > CLTF. This order of reactivity shows that the reactivity of these chlorobenzenes is suppressed by the electron-withdrawing substituents in the *para*-position This HDC reactivity is in contrast with that on the Pd/C catalyst [19], on which the reactivity of CLBN, CLAP and DCLB were also accelerated in a similar manner to the chlorobenzenes with electron-donating substituents.

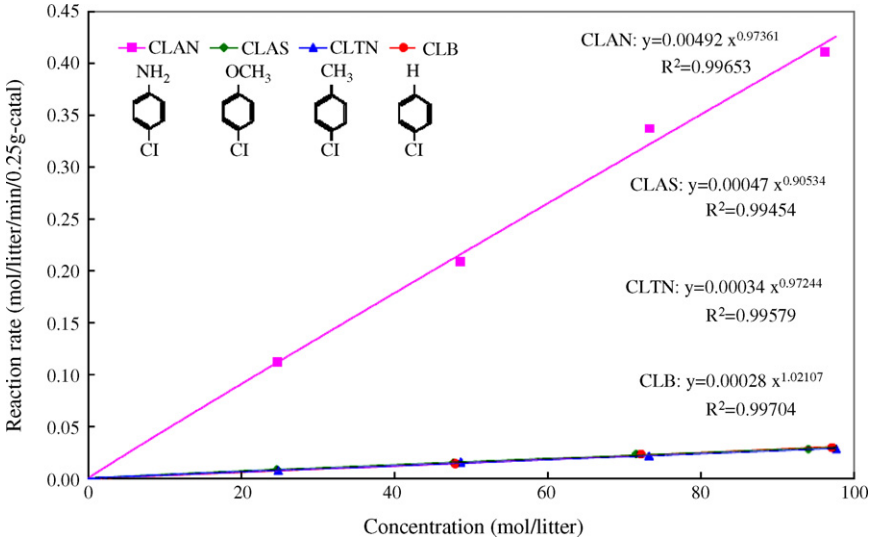

Fig. 4. Reaction rates of chlorobenzene and the *para*-isomers of chloroaniline, chloroanisole and chlorotoluene.

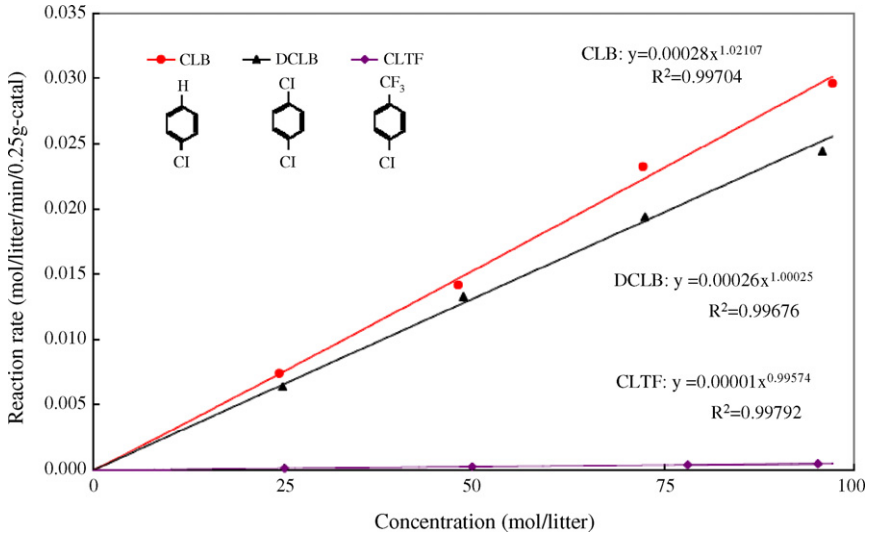

Fig. 5. Reaction rates of chlorobenzene and the *para*-isomers of dichlorobenzene and chlorobenzene trifluoride.

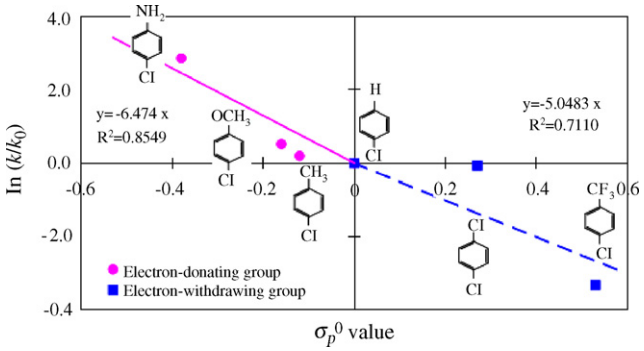

Fig. 6. Plots of the HDC reaction rate constant of the *para*-substituted chlorobenzenes to the substitution constant (σ_p^0).

In order to evaluate the electronic effect of the substituents quantitatively, the following Hammett equation [58,59] was applied to the above results:

$$\ln\left(\frac{k}{k_0}\right) = \rho\sigma$$

where k is the HDC reaction rate constant of the substituted chlorobenzenes; k_0 the HDC reaction rate constant of chlorobenzene; ρ the reaction constant; σ is Hammett's substitution constant. Although the correlation coefficient squares (R^2) for the two series of chlorobenzenes were somewhat low, correlations between the HDC rate constant and the substitution constant σ_p^0 were observed as shown in Fig. 6. A slightly larger absolute value of ρ for the chlorobenzenes with electron-donating substituents than for chlorobenzenes with electron-withdrawing substituents suggests a relatively higher sensitivity of the former to the electronic-effect of the substituent [59]. Furthermore, the negative ρ values suggest that HDC of *para*-substituted chlorobenzenes with electron-donating and -withdrawing substituents is an electrophilic reaction at the reaction center.

In the sequence of CLAN, CLAS, CLTN and CLB, thereby, the interaction between the chlorine atom of chlorobenzenes and the catalytic surface is expected. The same tendency to the HDC reactivity has been reported in the reaction of chlorobenzenes on the supported Ni catalyst in the gas phase reaction [3,9–11]. In the case of chlorobenzenes possessing the electron-withdrawing substituent, on the other hand, the negative ρ value suggests that the reaction occurs in the vicinity of the *para*-substituents. This prediction is supported from the products distributions in CLBN and CLAP (Table 2), where hydrogenolysis of the substituents proceeded mainly rather than the reductive cleavage of the Cl–C bond. In the reaction of the *para*-isomer of nitro (NO_2)-substituted chlorobenzene on the supported Ni catalyst, Wu et al. [16] have observed that the *para*-isomer was not hydrodechlorinated but hydrogenated at the NO_2 position and produced chloroaniline, suggesting that the benzene ring stand up from the catalytic surface with the electron-withdrawing substituents as an anchor. The order of the HDC reactivity (CLB > DCLB > CLTF) is also consistent with our present result.

In the next section, using molecular orbital method, we will try to clarify the factors affecting the HDC reactivity.

3.3. Molecular orbital calculation

3.3.1. Adsorption state

In order to obtain theoretical information on HDC reactivity, both the adsorption geometry and the adsorption energy of chlorobenzenes on the catalytic model of the Pt_{14} unit cell were calculated using the DFT method (Gaussian03W: B3LYP/LANL2DZ).

When the chlorobenzenes were placed on the center platinum atom of the (0 0 1) plane of the Pt_{14} clusters through the chlorine atom (named "Type-I" adsorption) (Fig. 7A), the atomic distance of Cl–Pt was lengthened from 0.20 to 0.877 nm (Fig. 7B).

On the other hand, when CLB was placed on the corner platinum atom of the (0 0 1) plane through the chlorine atom (named "Type-II" adsorption) (Fig. 8A), a high stable point was obtained (Fig. 8B).

When the adsorption energy (E_{ad}) of the chlorobenzenes was defined as below, as shown in Fig. 8, an interesting result was obtained in Type-II adsorption:

$$E_{ad} = E_{complex} - (E_{CLBs} + E_{Pt_{14}})$$

where $E_{complex}$ is the total energy in the optimized geometry of the "CLB–Pt_{14}" complex; E_{CLBs} the total energy in the

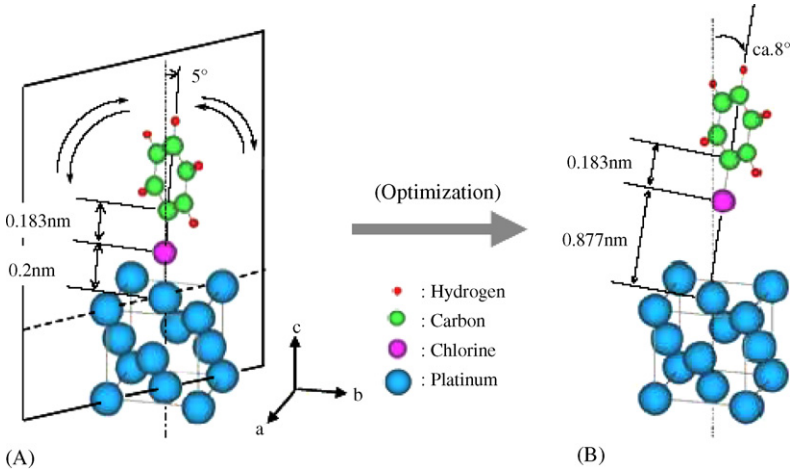

Fig. 7. (A) Initial and (B) final geometries for the adsorption of chlorobenzene on the center Pt atom of (0 0 1) plane in Pt_{14} cluster ("Type-I" adsorption).

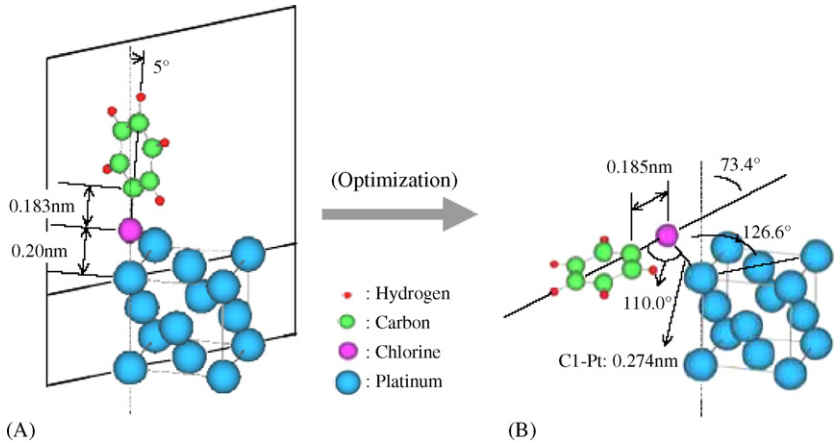

Fig. 8. (A) Initial and (B) final geometries for the adsorption of chlorobenzene on the corner Pt atom of (0 0 1) plane in Pt_{14} model cluster ("Type-II" adsorption).

optimized geometry of each chlorobenzene; $E_{Pt_{14}}$ is the total energy in the single point calculation of the Pt_{14} cluster, respectively.

Concerning the substituted chlorobenzenes with electron-donating substituents (the four red circles on the left in Fig. 9), the magnitude (absolute value) of E_{ad} decreased in the order of CLAN > CLAS ≥ CLTN ≥ CLB. This order is consistent with that of HDC reactivity. As for the chlorobenzenes with electron-withdrawing substituents (the two red circles on the right in Fig. 9), in contrast, the order of magnitude (absolute value) of E_{ad} differed from that of HDC reactivity. However, a reasonable order of E_{ad}, that is CLB > DCLB > CLTF, for this series of chlorobenzenes was observed when CLTF was adsorbed on the corner platinum atom through the *para*-substituent (the blue lozenge of the right extremity in Fig. 9). Although further studies are needed to confirm the adsorption geometry of CLTF, the Rideal–Eley reaction mechanism [60] may be presumed because the chlorine atom is located in the gas phase, far from the catalytic surface.

The role of the catalyst is generally assumed to lower the activation energy synergistically while increasing the collision number between two reactants on the catalytic surface, thereby causing an increase in the reaction rate [61]. For the HDC reaction, few studies have focused on chemical reactivity in relation to adsorption energy in spite of the fact that adsorption is crucially important. In the present study, the agreement of the order of adsorption energy with that of the experimental HDC reactivity may suggest that HDC reactivity is influenced by the difference in the affinity of reactants (that is, the affinity of the chlorine atom in the ultimate sense) onto the platinum atom of the catalytic surface.

3.3.2. *Orbital interactions*

To elucidate the electronic factors that affected adsorption stability, for Type-II adsorption state, the features of the interaction between chlorobenzenes and Pt_{14} model clusters were checked from the viewpoint of the energy levels of both the cluster and the molecules interacting with each other.

In the orbital interactions between chlorobenzenes and the Pt_{14} cluster, in every case, the degenerated LUMO ($E = -0.1798$ eV) of the cluster was predicted to play an important role as a partner orbital of the organic molecule. As seen

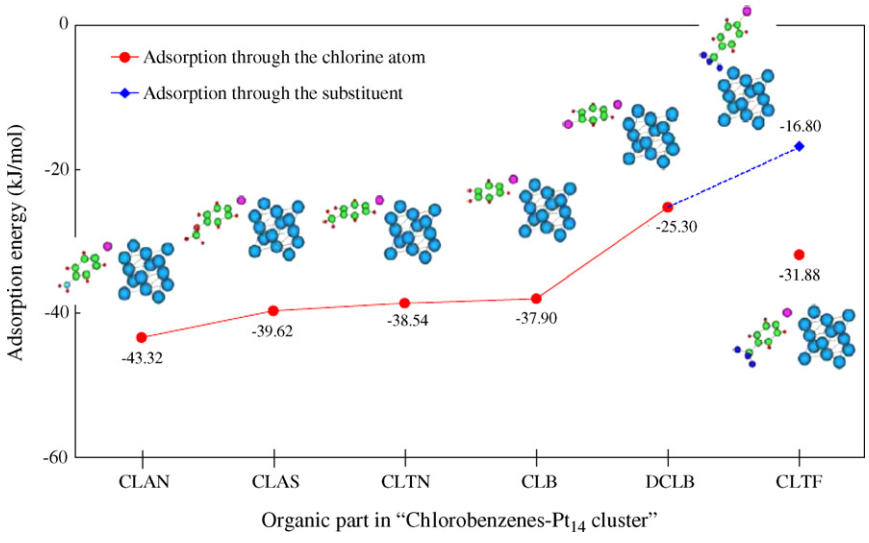

Fig. 9. Adsorption energy of chlorobenzenes on the Pt_{14} cluster for Type-II adsorption.

Table 3
Orbitals of chlorobenzenes interacting with LUMO of the Pt_{14} cluster and their energy levels

	CLAN	CLAS	CLTN	CLB	DCLB	CLTF
Interacting orbital	HOMO-3	HOMO-3	HOMO-2	HOMO-2	HOMO-2	HOMO-2
Energy (eV)	−0.3027	−0.3110	−0.3105	−0.3139	−0.3231	−0.3353

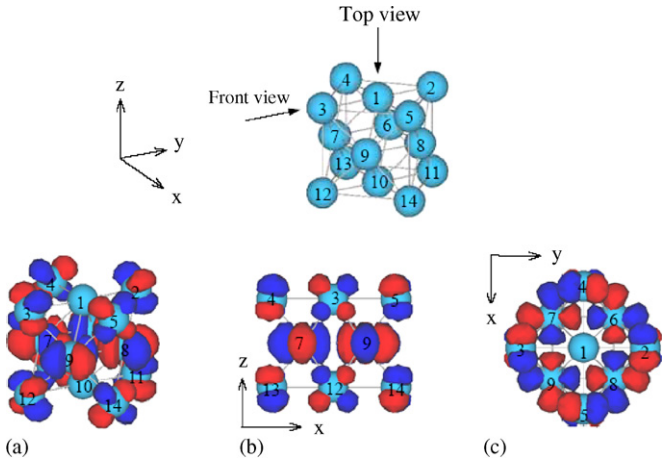

Fig. 10. Shape of degenerated LUMO: (a) over view; (b) front view; (c) top view.

in Fig. 10, this molecular orbital of the cluster consisted of d_{xz} atomic orbital of the corner atoms (nos. 2–5, 11–14 in Fig. 10) and $d_{x^2-y^2}$ atomic orbital of the face centered atoms (nos. 6–9 in Fig. 10). On the other hand, HOMO-2 or HOMO-3 of the organic part was expected to interact with the LUMO. The shape of these orbitals in the chlorobenzenes and their energy levels are shown in Table 3 and Fig. 11.

When a molecular axis of the chlorobenzenes was included in the Y–Z plane, and a molecular plane was orthogonalized to the Y–Z plane, as seen in Fig. 11, the p_x orbital on the chlorine atom was characteristic in all of the chlorobenzenes. Furthermore, a node was observed between the p_x orbital on the chlorine atom and the p_x orbital on the carbon atom of the benzene ring in these chlorobenzenes.

As a result of the interaction between (HOMO-3) of CLAN and the degenerated LUMO of the cluster, for example, (HOMO-62) ($E = -0.3488$ eV) as a bonding orbital and (LUMO + 3) ($E = -0.1296$ eV) as an antibonding orbital were generated. This is shown in Fig. 12. For the bonding orbital (HOMO-62), as seen in Fig. 13, the p_x orbital on the chlorine atom of the organic part was overlapped by the same phase as the d_{xz} orbital on the corner platinum atom (no. 3) of the cluster. This shows that the Cl–Pt bond is reinforced whereas the Cl–C bond is weakened. Also in the case of other chlorobenzenes, (HOMO-2) or (HOMO-3) was assigned as the interacting orbital of the organic part with the LUMO of the cluster.

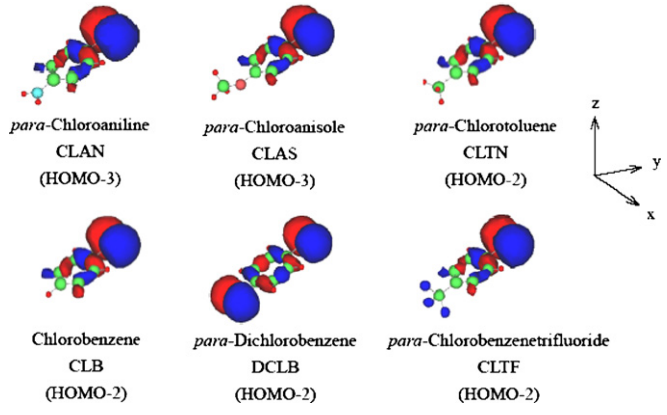

Fig. 11. Shape of interacting orbitals for chlorobenzene and the *para*-substituted chlorobenzenes.

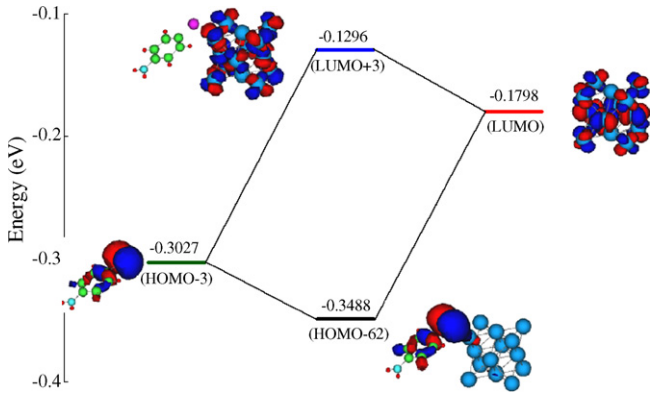

Fig. 12. The orbital interaction between (HOMO-3) of CLAN and (LUMO) of Pt_{14} cluster.

Furthermore, the calculated energy gaps (ΔE in Fig. 14) between the occupied orbitals in the chlorobenzenes and the degenerated LUMO in the Pt_{14} cluster lead to an interesting observation. That is, the magnitude of this energy gap increased in the order of CLAN < CLTN ≤ CLAS < CLB < DCLB < CLTF

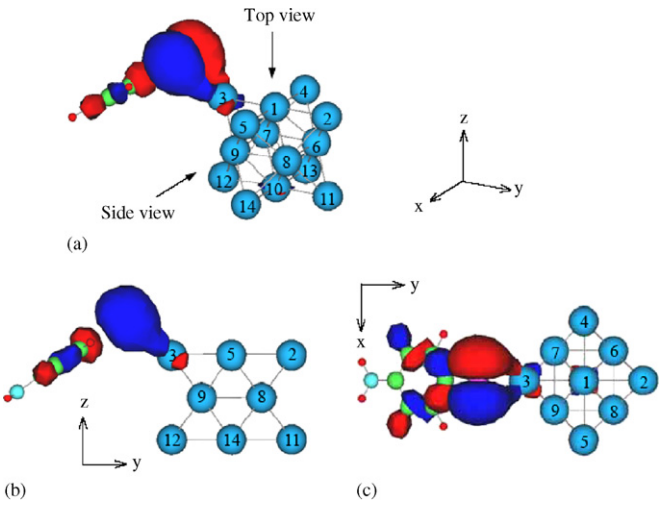

Fig. 13. (HOMO-62) orbital generated by the interaction between *para*-chloroaniline and Pt_{14} cluster: (a) over view; (b) side view; (c) top view.

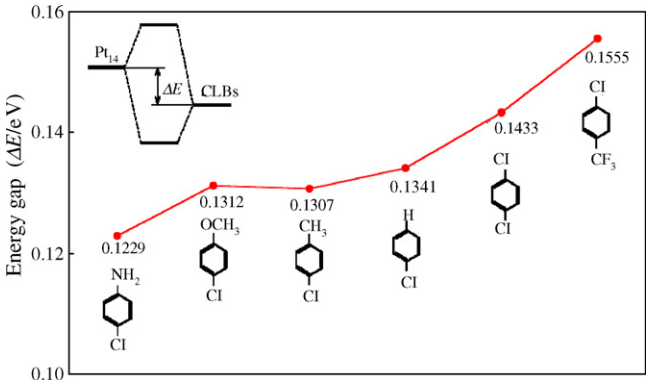

Fig. 14. Energy gaps between (HOMO-2) or (HOMO-3) of chlorobenzenes and LUMO of Pt_{14} cluster.

(Fig. 14). Since orbitals with smaller energy gaps generally interact more easily [62], HDC reactivity is expected to decrease in the opposite order to that of the energy gaps: CLAN > CLTN ≥ CLAS > CLB > DCLB > CLTF. Except for the reverse order between CLTN and CLAS, this order is the same as that of the HDC reactivity. Although further investigations are required to better interpret the HDC reaction mechanism, it may be deduced that the difference in HDC reactivity among substituted chlorobenzenes over the Pt/C catalyst was caused by the difference in energy gaps.

In the catalytic HDC of chlorobenzenes, dissociative adsorption following the formation of the σ-complex is reported in the literature [63]. Our final purpose in MO calculation is also to examine such evidence.

Although dissociative adsorption was not observed in the present calculation, in fact, the C–Cl bond length in the chlorobenzenes was expanded slightly; in addition, relationships between the HDC reactivity and the magnitude of adsorption energy were observed. Therefore, we regarded the present results as suggesting the importance of the adsorption.

However, we are now studying the dissociative adsorption state of chlorobenzenes accompanying the behavior of the surface hydrogen molecule/atoms.

4. Conclusion

1. In the hydrodechlorination (HDC) of chlorobenzene and *para*-substituted chlorobenzenes with electron-donating substituents over a 5%-Pt/C catalyst, the reductive cleavage of the carbon–chlorine bond proceeded selectively.
2. In the case of chlorobenzenes with electron-withdrawing substituents, whether the reductive cleavage of the carbon–chlorine bond (that is HDC) or the hydrogenolysis of the *para*-substituent took place depended on the electronic properties of the substituents. That is, the former reaction occurred in the reaction of the *para*-chloro and -trifluoromethyl-substituted chlorobenzenes, and the latter occurred in the reaction of the *para*-cyano and -acetyl-substituted chlorobenzenes.
3. Comparison with the reaction rate constants confirmed that the HDC of chlorobenzenes with electron-donating substituents was enhanced by the presence of the substituent, whereas for chlorobenzenes with electron-withdrawing substituents such as *para*-chloro and -trifluoromethyl substituents, HDC was suppressed by the substituent.
4. Concerning the effect of the substituents on HDC reactivity, a correlation between the rate constants and the Hammett substitution values (σ_p^0) was observed in both series of substituted chlorobenzenes although the square of correlation coefficients (R^2) was low.
5. The order of magnitude of the adsorption energy for the chlorobenzenes on the Pt_{14} model cluster, which was calculated using the DFT method (B3LYP/LANL2DZ), was consistent with that of HDC reactivity.
6. The difference in energy gaps between the degenerated LUMO of the Pt_{14} cluster and (HOMO-2) or (HOMO-3) of the chlorobenzenes was assumed to account for the adsorption stability.

Acknowledgements

We would like to thank Dr. Seiichi Takase for his useful advice on the molecular orbital method. We also wish to express our appreciation to Mr. Koshiro Koizumi for his assistance with the experiment.

References

[1] A.R. Suzdorf, S.V. Morozov, N.N. Anshits, S.I. Tsiganova, A.G. Anshits, Catal. Lett. 29 (1994) 49.
[2] V. de Jong, R. Louw, Appl. Catal. A: Gen. 271 (2004) 153.
[3] M.A. Keane, G. Pina, G. Tavoularis, Appl. Catal. B: Environ. 48 (2004) 275.
[4] K.V.R. Chary, K.S. Lakshmi, P.V.R. Roa, K.S.R. Rao, M. Papadaki, J. Mol. Catal. A: Chem. 223 (2004) 353.
[5] Y. Cesteros, P. Salagre, F. Medina, J.E. Sueiras, Catal. Lett. 79 (2002) 83.
[6] K.V.R. Chary, K.S. Lakshmi, M.R.V.S. Murthy, K.S.R. Rao, M. Papadaki, Catal. Commun. 4 (2003) 531.
[7] M.A. Keane, D.Y. Murzin, Chem. Eng. Sci. 56 (2001) 3185.
[8] I.V. Mishakov, V.V. Chesnokov, R.A. Buyanov, N.A. Pakhomov, Kinet. Catal. 42 (2001) 598.
[9] K.V. Murthy, P.M. Patterson, M.A. Keane, J. Mol. Catal. A: Chem. 225 (2005) 149.
[10] M.A. Keane, Appl. Catal. A: Gen. 271 (2004) 109.
[11] C. Menini, C. Park, E.J. Shin, G. Tavoularis, M.A. Keane, Catal. Today 62 (2000) 355.
[12] Y. Hashimoto, Y. Uemichi, A. Ayame, Appl. Catal. A: Gen. 287 (2005) 89.
[13] F. Gioia, E.J. Gallagher, V. Famiglietti, J. Hazard. Mater. 38 (1994) 277.
[14] F. Murena, Environ. Technol. 18 (1997) 317.
[15] W. Wu, J. Xu, Catal. Commun. 5 (2004) 591.
[16] W. Wu, J. Xu, R. Ohnishi, Appl. Catal. B: Environ. 60 (2005) 129.
[17] E. López, S. Ordóñez, F.V. Díez, H. Sastre, Stud. Surf. Sci. Catal. 133 (2001) 521.
[18] F.J. Urbano, J.M. Marinas, J. Mol. Catal. A: Chem. 173 (2001) 329.
[19] K. Konuma, N. Kameda, J. Mol. Catal. A: Chem. 178 (2002) 239.
[20] R. Gopinath, K. Narasimha Rao, P.S. Sai Prasad, S.S. Madhavendra, S. Narayanan, G. Vivekanandan, J. Mon. Catal. A: Chem. 181 (2002) 215.
[21] M.A. Aramendía, V. Voráu, I.M. García, C. Jiménez, F. Lafont, A. Marinas, J.M. Marinas, F.J. Urbano, J. Mol. Catal. A: Chem. 184 (2002) 237.
[22] R. Gopinath, N. Lingaiah, B. Sreedhar, I. Suryanarayana, P.S.S. Prasad, A. Obuchi, Appl. Catal. B: Environ. 46 (2003) 587.
[23] G. Yuan, M.A. Keane, Chem. Eng. Sci. 58 (2003) 257.
[24] T. Janiak, J. Błażejowski, Appl. Catal. A: Gen. 271 (2004) 103.
[25] F. Murena, F. Gioia, Appl. Catal. A: Gen. 271 (2004) 145.

[26] S.S. Zinovyev, N.A. Shinkova, A. Perosa, P. Tundo, Appl. Catal. B: Environ. 55 (2005) 39.
[27] J.M. Moreno, M.A. Aramendía, A. Marinas, J.M. Marinas, F.J. Urbano, Appl. Catal. B: Environ. 59 (2005) 275.
[28] F.-D. Kopinke, K. Mackenzie, R. Koehler, A. Georgi, Appl. Catal. A: Gen. 271 (2004) 119.
[29] P.D. Vaidya, V.V. Mahajani, Appl. Catal. B: Environ. 51 (2004) 21.
[30] E.J. Creyghton, M.H.W. Burgers, J.C. Jansen, H. van Beckkum, Appl. Catal. A: Gen. 128 (1995) 275.
[31] S.T. Srinivas, L.J. Lakshmi, N. Lingaiah, P.S.S. Prasad, P.K. Rao, Appl. Catal. A: Gen. 135 (1996) L201.
[32] P. Dini, J.C.J. Bart, N. Giordano, J.C.S. Perkin II (1975) 1479.
[33] S.T. Srinivas, P.S.S. Prasad, S.S. Madhavendra, P.K. Rao, Stud. Surf. Sci. Catal. 113 (1998) 835.
[34] S.T. Srinivas, P.S.S. Prasad, P.K. Rao, Catal. Lett. 50 (1998) 77.
[35] Y. Hashimoto, A. Ayame, Appl. Catal. A: Gen. 250 (2003) 247.
[36] H. Yin, Y. Wada, T. Kitamura, S. Yanagida, Environ. Sci. Technol. 35 (2001) 227.
[37] M. Julliard, M. Chanon, J. Photochem. Photobiol. A: Chem. 83 (1994) 107.
[38] N. Ohtsuka, K. Minomo, S. Hosono, Y. Kurata, M. Sugisaki, Organohalogen Compd. 52 (2001) 405.
[39] A.T. Soltermann, J.J. Cosa, C.M. Previtali, J. Photochem. Photobiol. A: Chem. 60 (1991) 111.
[40] J.G. Rodríguez, A. Lafuente, Tetrahedron Lett. 43 (2002) 9645.
[41] A. Tiehm, I. Kohnagel, U. Neis, Water Sci. Technol. 43 (2001) 297.
[42] O. Kranz, J. Voss, Chem. Sci. 58 (2003) 1187.
[43] H. Cheng, K. Scott, P.A. Christensen, J. Electroanal. Chem. 566 (2004) 131.
[44] I.-M. Chen, B.-V. Chang, S.-Y. Yuan, Y.-S. Wang, Water Air Soil Pollut. 139 (2002) 61.
[45] U.R. Pillai, E.S. Demessie, R.S. Varma, Green Chem. 6 (2004) 295.
[46] H. Yin, Y. Wada, T. Kitamura, T. Sakata, H. Mori, S. Yanagida, Chem. Lett. 4 (2001) 334.
[47] G.A. Zacheis, K.A. Gray, P.V. Kamat, J. Phys. Chem. B 105 (2001) 4715.
[48] J.B. Foresman, A.E. Frisch, Exploring Chemistry with Electronic Structure Methods, 2nd ed., Gaussian Inc., Pittsburgh, PA, 1996, pp. 118, 272 and 282.
[49] A.E. Frisch, M.J. Frisch, G.W. Trucks, Gaussian03 User's Reference, Gaussian Inc., Pittsburgh, PA, 2003, p. 73.
[50] A.D. Becke, J. Chem. Phys. 98 (1993) 5648.
[51] C. Lee, W. Yang, R.G. Parr, Phys. Rev. B 37 (1988) 785.
[52] B. Meihelich, A. Savin, H. Stoll, H. Preuss, Chem. Phys. Lett. 157 (1989) 200.
[53] A.E. Frisch, M.J. Frisch, G.W. Trucks, Gaussian03 User's Reference, Gaussian Inc., Pittsburgh, PA, 2003, p. 24.
[54] P.J. Hay, W.R. Wadt, J. Chem. Phys. 82 (1985) 270.
[55] W.R. Wadt, P.J. Hay, J. Chem. Phys. 82 (1985) 284.
[56] P.J. Hay, W.R. Wadt, J. Chem. Phys. 82 (1985) 299.
[57] H. Adachi, M. Tsukada, C. Satoko, J. Phys. Soc. Jpn. 45 (1978) 875.
[58] N. Inamoto, Hammett-Soku, Maruzen, Tokyo, 1983, p. 20.
[59] H. Iwamura, R. Noyori, T. Nkai, I. Kitagawa (Eds.), Daigakuin Yuukikagaku (jou), Koudansha, 1988, p. 260.
[60] C.N. Satterfield, Heterogeneous Catalyst in Practice, McGraw-Hill, 1980, p. 53.
[61] B. Cornils, W.A. Herrmann, R. Schögl, C.-H. Wong (Eds.), Catalysis from A to Z (Second, Completely Revised and Enlarged Edition), Wiley–VCH Verlag GmbH & Co., KGaA, Weinheim, 2003, p. 10.
[62] R. Hoffmann, Solid and Surfaces, Wiley–VCH Inc., Canada, 1988, p. 66.
[63] Yu.A. Serguchev, Yu.V. Belokpytov, Kinet. Catal. 42 (2001) 195.